



OPEN

# PAWI-2 overcomes tumor stemness and drug resistance via cell cycle arrest in integrin $\beta_3$ -KRAS-dependent pancreatic cancer stem cells

Jiongjia Cheng<sup>✉</sup> & John R. Cashman

Today, pancreatic cancer (PC) remains a major health problem in the US. The fact that cancer stem cells (CSCs) become enriched in humans following anti-cancer therapy implicates CSCs as key contributors to tumor dormancy, metastasis, and relapse in PC. A highly validated CSC model (FG $\beta_3$  cells) was used to test a novel compound (PAWI-2) to eradicate CSCs. Compared to parental bulk FG cells, PAWI-2 showed greater potency to inhibit cell viability and self-renewal capacity of FG $\beta_3$  cells. For FG $\beta_3$  cells, dysregulated integrin  $\beta_3$ -KRAS signaling drives tumor progression. PAWI-2 inhibited  $\beta_3$ -KRAS signaling independent of KRAS. This is clinically relevant. PAWI-2 targeted the downstream TBK1 phosphorylation cascade that was negatively regulated by optineurin phosphorylation via a feedback mechanism. This was confirmed by TBK1 genetic knockdown or co-treatment with TBK1-specific inhibitor (MRT67307). PAWI-2 also overcame erlotinib (an EGFR inhibitor) resistance in FG $\beta_3$  cells more potently than bortezomib. In the proposed working model, optineurin acts as a key regulator to link inhibition of KRAS signaling and cell cycle arrest (G2/M). The findings show PAWI-2 is a new approach to reverse tumor stemness that resensitizes CSC tumors to drug inhibition.

Pancreatic cancer (PC) remains a major health problem in the US and soon will be the second most common cause of mortality due to cancer<sup>1,2</sup>. One of the only curable treatment options for PC is surgical resection<sup>3</sup>. However, disease recurrence is still at high risk after surgery and a majority of post-surgical patients develop advanced metastatic disease, thus necessitating chemo- and radiation therapies<sup>4</sup>. Front-line chemotherapies cause serious side effects<sup>5-7</sup>. A majority of PC patients are often resistant to clinical therapies<sup>4</sup>. Thus, it remains a challenge to develop an efficacious clinically useful PC therapy.

Cancer stem cells (CSCs) are hallmarks of cancer and inherently resistant to medical therapy<sup>8,9</sup>. CSCs become enriched in humans following chemo- or radiotherapy. This implicates CSCs as key contributors to tumor dormancy, metastasis, and relapse<sup>10,11</sup>. These functional features of CSCs make CSCs different from bulk tumor cells and enable CSCs to initiate and maintain tumor development from tumor cells present in a malignant tumor<sup>12,13</sup>.

CSCs were identified and prospectively isolated from a number of solid tumors by using CSC-specific biomarkers<sup>12,13</sup>. These biomarkers show a distinct cell population with increased renewal capacity and the ability to recapitulate heterogeneity, multi-lineage differentiation and long-term repopulation<sup>12,13</sup>. One cell surface adhesion molecule (i.e., integrin  $\alpha_v\beta_3$ ) is well-established as a driver of tumor progression due to association with greater incidence of metastasis<sup>14,15</sup>. This occurs in a variety of cancers<sup>15-17</sup>. The capability of integrin  $\alpha_v\beta_3$  to trigger anchorage-independent cell survival and tumor metastasis<sup>14,18,19</sup> shows that integrin  $\alpha_v\beta_3$  expression is a biomarker/functional contributor to CSC progression and drug resistance. Human pancreatic cancer stem cells (hPCSCs) reported previously (i.e., FG $\beta_3$  cells) are a validated human CSC model<sup>19-21</sup> that overexpresses integrin  $\alpha_v\beta_3$ . In FG $\beta_3$  cells, integrin  $\alpha_v\beta_3$  recruits Kirsten rat sarcoma viral oncogene homologue GTPase (KRAS) and RAS Like Proto-Oncogene B (RalB) to activate serine/threonine kinase Tank-binding kinase 1 (TBK1, I $\kappa$ B kinase (IKK)-related kinase) and nuclear factor kappa-light-chain-enhancer of activated B cells (NF- $\kappa$ B) to trigger

Human BioMolecular Research Institute and ChemRegen, Inc., San Diego, CA, 92121, USA. ✉e-mail: [jcheng@hbri.org](mailto:jcheng@hbri.org)

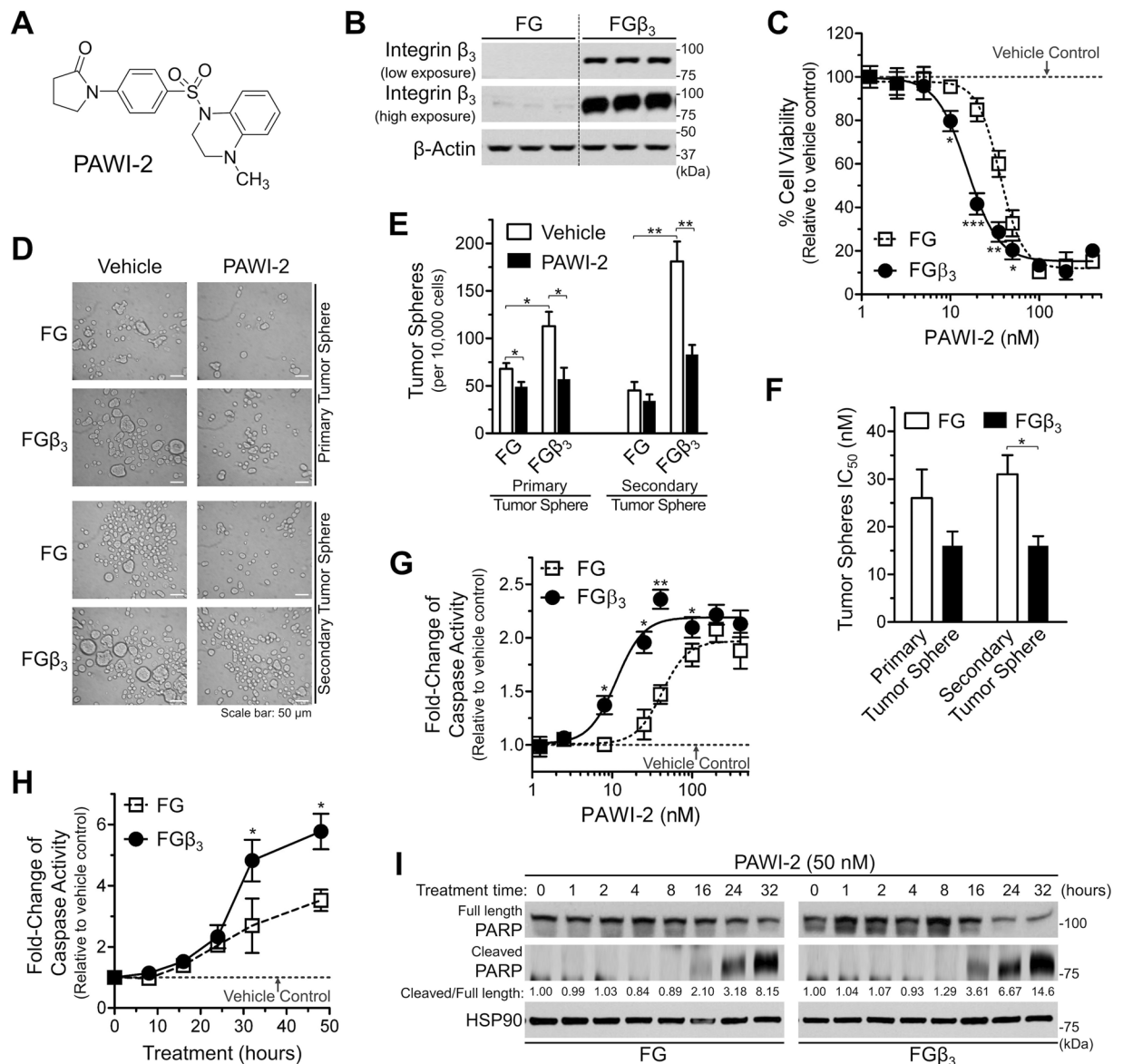


**Figure 1.** PAWI-2 overcomes tumor stemness driven by integrin  $\beta_3$  expression. (A) Chemical structure of PAWI-2. (B) Overexpression of integrin  $\beta_3$  in FG $\beta_3$  cells (with human  $\beta_3$ /pcDNA3.1 vector) compared to parental FG cells (with empty vector). (C) Dose-dependent effect of PAWI-2 on inhibition of cell viability in FG and FG $\beta_3$  cells. (D–F) Effect of PAWI-2 on the inhibition of primary and secondary tumor sphere formation in FG and FG $\beta_3$  cells: (D) representative tumor sphere images; (E) self-renewal capacity measured by quantifying the number of primary and secondary tumor spheres; (F) bar graph of the half-maximum inhibitory concentrations (IC<sub>50</sub>s). (G–I) Effect of PAWI-2 on activation of cell apoptosis in FG and FG $\beta_3$  cells: (G) dose-dependent and (H) time-dependent activation of caspase-3/7 activity by PAWI-2 determined by Caspase-Glo 3/7 assay; (I) immunoblot analyses of PARP (full length) and cleaved PARP as determined with whole-cell extracts. Concentration of PAWI-2 used were as indicated: 1.2–400 nM in C, G, 20 nM in D, E and 50 nM in H, I; treatment time used was as indicated: 72 hours in C, 24 hours in D–G, 0–48 hours in H and 0–32 hours in I; vehicle control (0.5% DMSO).  $\beta$ -Actin or HSP90 were used as loading controls in B, I. Data were mean  $\pm$  SD (n = 3) in C, E–H; P-values were estimated by Student *t* tests in C, E–H (\**P* < 0.05, \*\**P* < 0.01, \*\*\**P* < 0.001). The full-length blots are presented in Supplementary Fig. S7.

disregulated KRAS-RalB-NF- $\kappa$ B. This pathway was reported to be a pharmacological target to reverse CSC-like properties or re-sensitize drug resistance for established FG $\beta_3$  tumors<sup>19–21</sup>.

Given the important role of hPCSCs, a novel treatment strategy that targets hPCSCs or their extrinsic and intrinsic regulators could be of significant clinical utility to treat PC. Herein, we report PAWI-2 (Fig. 1A) that kills drug-resistant hPCSCs (i.e., FG $\beta_3$  cells) and synergizes erlotinib by targeting optineurin (OPTN)-dependent cell cycle arrest. Development of PAWI-2 as an anti-PC drug candidate addresses an unmet clinical need. PAWI-2 may also improve standard of care for patients because it synergizes eradication of hPCSCs.

## Results

**Effect of PAWI-2 on cell viability and self-renewal capacity of FG $\beta_3$  cells.** FG $\beta_3$  cells were generated by stable transfection of fast-growing (FG) human PC cells with human  $\beta_3$ /pcDNA3.1<sup>19</sup>. FG $\beta_3$  cells possessing CSC-like properties have an elevated expression of integrin  $\beta_3$  compared to parental, bulk FG cells (Fig. 1B). PAWI-2 was two-fold more potent to inhibit cell viability (Supplemental Table S1, Fig. 1C) of FG $\beta_3$  cells (IC<sub>50</sub>, 15 nM) compared to FG cells (IC<sub>50</sub>, 36 nM). FG $\beta_3$  cells showed four-fold increased self-renewal capacity (i.e., secondary tumor sphere formation mediated by integrin  $\beta_3$ ) relative to FG cells (Fig. 1D–F). PAWI-2 (20 nM) inhibited self-renewal capacity two-fold in FG $\beta_3$  cells (Fig. 1E). *In vitro*, PAWI-2 was two-fold more effective to inhibit self-renewal capacity of FG $\beta_3$  (IC<sub>50</sub>, 16 nM) compared to FG cells (IC<sub>50</sub>, 31 nM) (Fig. 1F, Supplemental Table S1).

**Effect of PAWI-2 on induction of mitochondrial-controlled apoptosis.** PAWI-2 potently (i.e., 5.9-fold relative to vehicle-control) activated apoptosis (i.e., activation of caspase-3/7, Fig. 1G,H) in FG $\beta_3$  cells (EC<sub>50</sub>, 11 nM, 48 hours). PAWI-2-mediated apoptosis was less apparent in FG cells (EC<sub>50</sub>, 42 nM; 3.5-fold increase). Selective potency of PAWI-2 was further shown by PARP cleavage. Compared to FG cells, induction of PARP cleavage was more apparent in FG $\beta_3$  cells (6.7- vs. 3.2-fold increase, respectively, at 24 hours; Fig. 1I). Similarly, apoptosis induced by PAWI-2 in FG and FG $\beta_3$  cells was controlled by ATM-mitochondrial p53-dependent apoptotic signaling. PAWI-2 activated upstream DNA-damage checkpoint via ATR/ATM-kinase activation (Supplemental Fig. S1A) and inhibited cytosolic p53/Bax binding to anti-apoptotic Bcl-xL (Supplemental Fig. S1B). This caused activation of pro-apoptotic p53/Bax and induced mitochondrial cytochrome c release to trigger cell apoptosis (Supplemental Fig. S1C). This mechanism of action has been observed for PAWI-2 in other non-CSC cancer cells<sup>22–25</sup>.

**Effect of PAWI-2 on downstream of the KRAS-NF- $\kappa$ B pathway.** In FG $\beta_3$  cells, overexpression of integrin  $\alpha_v\beta_3$  interacts with KRAS through galectin-3 to recruit KRAS and RalB to activate TBK1 and NF- $\kappa$ B that triggers dysregulated KRAS-RalB-NF- $\kappa$ B signaling<sup>19–21</sup>. This is the dominant mechanism to induce CSC-like properties in FG $\beta_3$  cells and causes drug resistance for established FG $\beta_3$  tumors. Accordingly, the effect of PAWI-2 on dysregulated integrin  $\alpha_v\beta_3$ -KRAS-NF- $\kappa$ B signaling in FG $\beta_3$  cells was studied. PAWI-2 neither caused disruption of KRAS interactions with other effectors (i.e., integrin  $\beta_3$ , galectin-3; Supplemental Fig. S2A) nor inhibited Ral GTPase (i.e., did not affect RalA/B-GTP, an active form of RalA/B; Supplemental Fig. S2B). PAWI-2 inhibited KRAS-NF- $\kappa$ B phosphorylation of TBK1 at Ser172 (pSer172-TBK1; Fig. 2A) without affecting other key components of this pathway (integrin  $\beta_3$ , KRAS, galectin-3, RalB and c-Rel were not affected by PAWI-2 up to 5  $\mu$ M; Supplemental Fig. S2C). PAWI-2 selectively inhibited phosphorylation of TBK1. Compared to FG cells (IC<sub>50</sub>, 92 nM), PAWI-2 inhibited phosphorylation of TBK1 (pSer172-TBK1/TBK1) 5-fold more potently in FG $\beta_3$  cells (IC<sub>50</sub>, 17 nM; Supplemental Fig. S2D), similar to other *in vitro* cell viability, self-renewal capacity, and cell apoptosis characterizations (10–40 nM; Fig. 1C,E,G; Supplemental Table S1).

Downstream interruption of KRAS-NF- $\kappa$ B signaling (i.e., inhibition of TBK1 with TBK1 shRNA; Fig. 2B–E) largely overcame integrin  $\beta_3$ -mediated stemness (i.e., less tumor sphere formation in FG $\beta_3$  cells with TBK1 knockdown; Fig. 2D). Treatment with PAWI-2 (10–20 nM) enhanced inhibition of TBK1 knockdown on cell viability (20% greater) and self-renewal capacity (44% greater) in FG $\beta_3$  cells (Fig. 2C,D). TBK1 can phosphorylate p62/sequestosome-1 (p62) at Ser403 and optineurin (OPTN) at Ser177<sup>26</sup>. However, after treatment with PAWI-2, both phosphorylation of p62 or OPTN were increased 2–5 fold in FG and FG $\beta_3$  cells (Fig. 2E). Genetic knockdown of TBK1 down-regulated phosphorylation of p62 but not autophosphorylation of TBK1 or phosphorylation of OPTN (pS172-TBK1 and pS177-OPTN, respectively, Fig. 2E).

Compared to cells treated with PAWI-2 alone, co-treatment with TBK1 kinase inhibitor (MRT67307)<sup>27</sup> and PAWI-2 enhanced inhibition of cell viability (30% greater; Supplemental Table S2; Fig. 2F) and self-renewal capacity (25% greater; Fig. 2G) in FG and FG $\beta_3$  cells. In FG $\beta_3$  cells, enhancement of cell killing with co-treatment with PAWI-2 and MRT67307 was not associated with induction of cell apoptosis. For example, in the presence of PAWI-2 and MRT67307, caspase activation and PARP cleavage was comparable to treatment of PAWI-2 alone (Supplemental Fig. S3A,B). The enhanced inhibition of cell viability and self-renewal capacity (Fig. 2F,G) was associated with OPTN phosphorylation (2–4 fold activation; Supplemental Fig. S3C) similar to the result observed in the genetic knockdown of TBK1 (2–5 fold activation; Fig. 2E). Moreover, pharmaceutical inhibition of TBK1 by MRT67307 also down-regulated phosphorylation of p62 (pS403-p62) but not pS172-TBK1 or pS177-OPTN (Supplemental Fig. S3C). This result showed that phosphorylation of p62 induced by PAWI-2 was most likely related to TBK1 activity but phosphorylation of OPTN may not be solely associated with TBK1 activity.

**Effect of PAWI-2 on OPTN phosphorylation in the presence of other inhibitors.** Integrin  $\beta_3$ -mediated self-renewal capacity is associated with drug resistance in FG $\beta_3$  cells<sup>19</sup>. Co-administration of erlotinib with proteasome inhibitor bortezomib was examined to determine effects on cell viability (Supplemental Table S2) and self-renewal capacity<sup>19,21</sup>. In FG $\beta_3$  cells, co-administration of “PAWI-2 and erlotinib” enhanced inhibition of erlotinib alone on cell viability (30% greater) and self-renewal capacity (80% greater), compared to co-administration of “erlotinib and bortezomib” (Fig. 3A,B). Chou-Talalay analysis of synergism or antagonism was calculated based on a dose-dependent inhibition of cell viability for drug alone or drug-drug combinations. Synergism or antagonism between drugs was defined by combination index (CI values), showing PAWI-2 synergized erlotinib (but antagonized bortezomib, CI values > 1; Table 1) with greater synergism for FG $\beta_3$  cells compared to FG cells (CI values < 1; Table 1). Synergism between “erlotinib and bortezomib” was observed in FG cells but was less apparent in FG $\beta_3$  cells (Table 1). Synergism of “PAWI-2 and erlotinib” paralleled induction of cell apoptosis (i.e., “PAWI-2 and erlotinib” enhanced activation of caspase and PARP cleavage compared to PAWI-2 or erlotinib alone; Supplemental Fig. S4A,B).

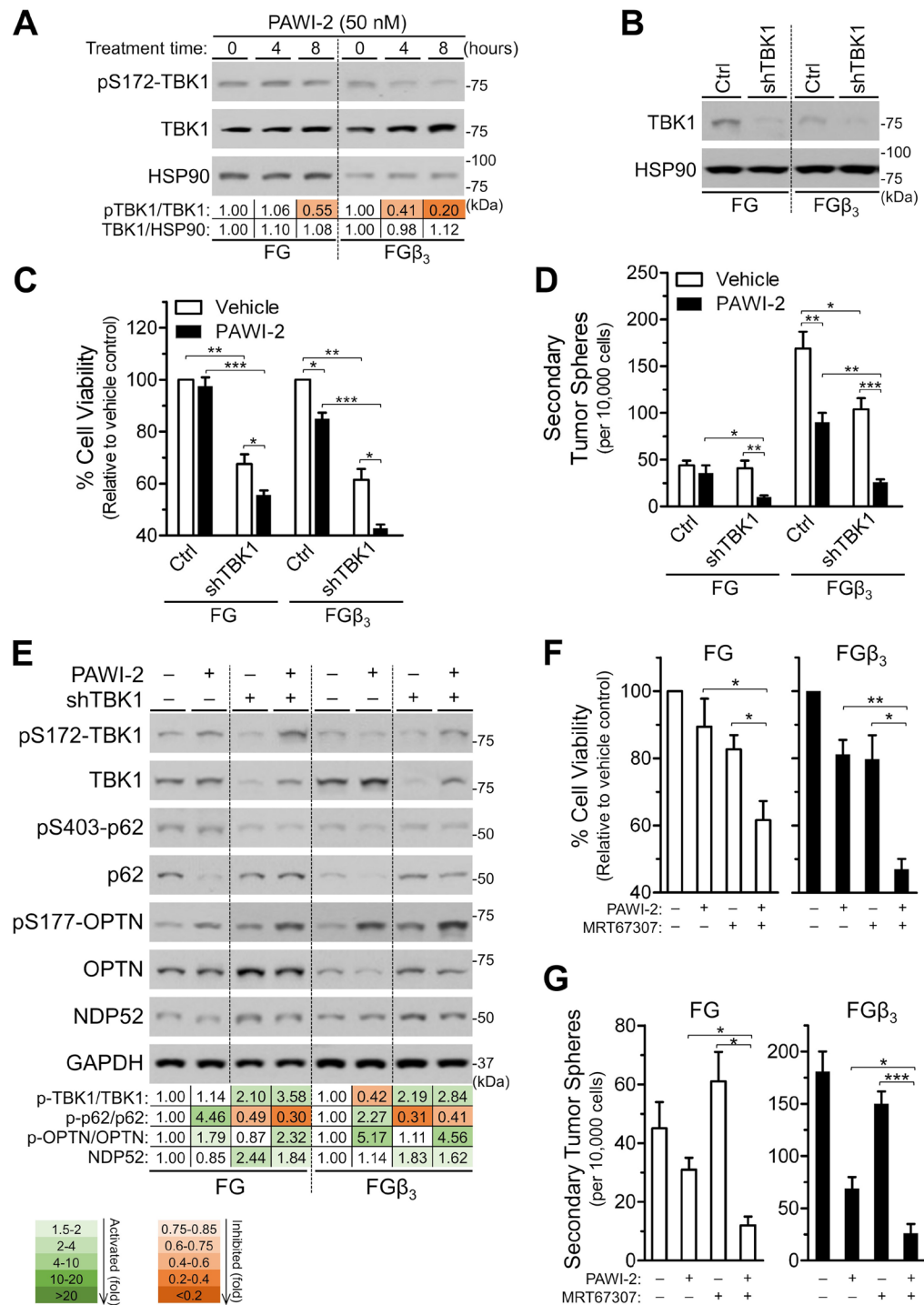


**Figure 2.** PAWI-2 affects KRAS-NF- $\kappa$ B signaling by targeting TBK1 phosphorylation to overcome tumor stemness. (A) Immunoblots and densitometry analysis of phospho-Ser172-TBK1 (pS172-TBK1) and TBK1 as determined with whole-cell extracts. (B--E) TBK1 knockdown enhanced the effect of PAWI-2 in FG and FG $\beta_3$  cells: (B) immunoblots show TBK1 genetic knockdown efficiency used in this study; effect of TBK1 knockdown (C) on cell viability inhibited by PAWI-2 as measured by a CellTiter-Glo assay and (D) effects on self-renewal capacity inhibited by PAWI-2 as measured by quantifying the number of secondary tumor spheres; (E) immunoblots and densitometry analysis of the effect of PAWI-2 on pS172-TBK1, TBK1, phospho-Ser403-p62 (pS403-p62), p62, phospho-Ser177-OPTN (pS177-OPTN), OPTN, or NDP52 in cells with TBK1 knockdown compared to control cells. (F,G) Enhancement of inhibition of (F) cell viability and (G) self-renewal capacity by co-treatment of PAWI-2 with TBK1 specific inhibitor (MRT67307, 1  $\mu$ M). Concentrations of PAWI-2 used were as indicated: 50 nM in A, E, 10 nM in C, F and 20 nM in D, G; treatment time used was as indicated: 0–16 hours in A, 24 hours in C, D, F, G and 8 hours in E; vehicle control (0.5% DMSO). GAPDH or HSP90 was used as a loading control in A, B, E. Data are mean  $\pm$  SD ( $n = 3$ ) in C, D, F, G;  $P$ -values were estimated by Student  $t$  tests in C, D, F, G (\* $P < 0.05$ , \*\* $P < 0.01$ , \*\*\* $P < 0.001$ ). The full-length blots are presented in Supplementary Fig. S7.

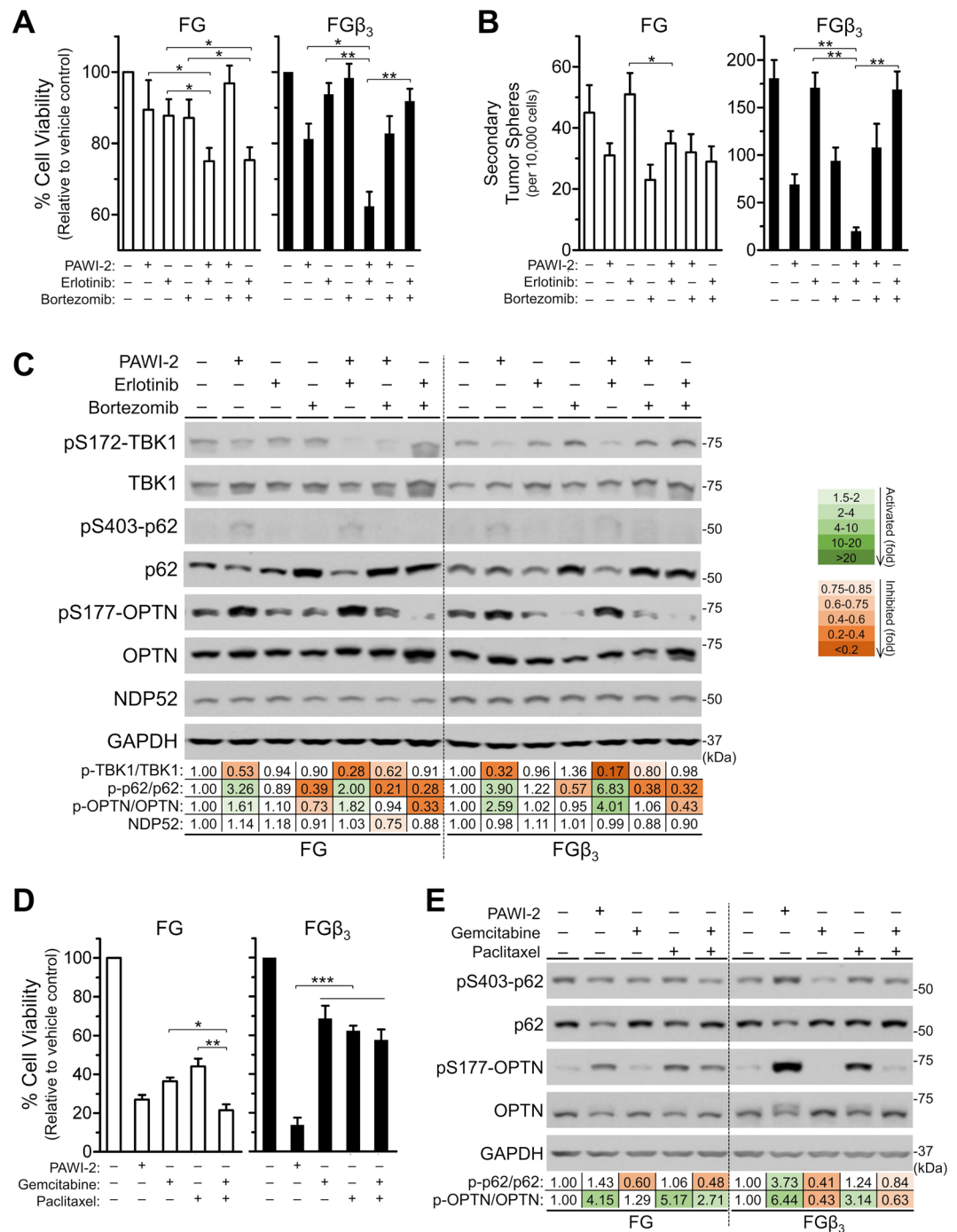


**Figure 3.** (A–C) PAWI-2 overcomes erlotinib resistance in FG $\beta_3$  cells. Inhibition of (A) cell viability and (B) self-renewal capacity (secondary tumor sphere formation) by EGFR inhibitor (erlotinib) in the presence of PAWI-2 is significantly enhanced compared to single agent treatment or combination of erlotinib (1  $\mu$ M) with proteasome inhibitor (bortezomib). (C) Immunoblots and densitometry analysis of the effect on phospho-Ser403-p62 (pS403-p62), p62, phospho-Ser177-OPTN (pS177-OPTN), OPTN, or NDP52 in FG and FG $\beta_3$  cells after co-treatment of PAWI-2 with erlotinib or bortezomib. (D) PAWI-2 is more effective than clinically-approved drug combinations of gemcitabine (25 nM) with paclitaxel (25 nM) in FG $\beta_3$  cells at inhibiting cell viability; (E) Immunoblots and densitometry analysis of the effect of gemcitabine or paclitaxel or in combination on pS403-p62, p62, pS177-OPTN, OPTN compared to PAWI-2 alone. Concentrations of PAWI-2 used were as indicated: 10 nM in A, 20 nM in B, 50 nM in C–E; concentrations of bortezomib used were as indicated: 10 nM in A, 20 nM in B, 50 nM in C; treatment time used was as indicated: 72 hours in A, D, 24 hours in B, 8 hours in C and 16 hours in E; vehicle control (0.5% DMSO). GAPDH was used as a loading control in C, E. Data are mean  $\pm$  SD (n = 3) in A, B, D; P-values were estimated by Student *t* tests in A, B, D (\**P* < 0.05, \*\**P* < 0.01, \*\*\**P* < 0.001). The full-length blots are presented in Supplementary Fig. S7.

Cell lines	Drug/Combo <sup>a</sup>	CI <sup>b</sup> values at different EDs <sup>c</sup>		
		ED <sub>75</sub>	ED <sub>90</sub>	ED <sub>95</sub>
FG	Erlotinib + Bortezomib	<b>0.51<sup>d</sup></b>	<b>0.56<sup>d</sup></b>	<b>0.59<sup>d</sup></b>
	Erlotinib + PAWI-2	<b>0.64<sup>d</sup></b>	<b>0.74<sup>d</sup></b>	<b>0.86<sup>d</sup></b>
	Bortezomib + PAWI-2	1.56	1.50	1.47
FG $\beta_3$	Erlotinib + Bortezomib	<b>0.87<sup>d</sup></b>	1.07	1.19
	Erlotinib + PAWI-2	<b>0.45<sup>d</sup></b>	<b>0.32<sup>d</sup></b>	<b>0.25<sup>d</sup></b>
	Bortezomib + PAWI-2	1.55	1.59	1.63

**Table 1.** Combination index (CI) values quantified synergism after treatment with PAWI-2 and erlotinib or bortezomib in FG and FG $\beta_3$  cells. <sup>a</sup>Ratios of Erlotinib:Bortezomib, Erlotinib:PAWI-2 and Bortezomib:PAWI-2 were 50:1, 50:1 and 1:1, respectively; <sup>b</sup>Combination Index (CI) values were calculated based on the Chou-Talalay method; values of CI < 1, = 1 and > 1 indicate synergism, additive and antagonism, respectively; <sup>c</sup>ED<sub>75, 90, 95</sub> represent concentrations that cause 75%, 90% and 95% of proliferation inhibition, respectively; <sup>d</sup>Bold values show synergy.

Bortezomib works on inhibition of late stage autophagy that promotes accumulation of p62<sup>28</sup>. However, in our hands, the effect of bortezomib on autophagy alone or in combination with erlotinib in FG and FG $\beta_3$  cells was modest (p62 and LC3 accumulation was < 2-fold; Fig. 3C, Supplemental Fig. S4C). The distinct pattern of changes of LC3-I to LC3-II was not significantly affected by co-treatment of PAWI-2 with erlotinib. This showed synergism of PAWI-2 with erlotinib was not dominated by an autophagy-related effect. Synergism between PAWI-2 and erlotinib and antagonism between PAWI-2 with bortezomib were highly correlated with OPTN phosphorylation based on a plot of CI values versus pS177-OPTN fold-change (correlation coefficient  $r^2 > 0.8$ ). Co-administration of erlotinib and PAWI-2 increased pS177-OPTN 4-fold in FG $\beta_3$  cells. In contrast, in the presence of PAWI-2 and bortezomib, OPTN phosphorylation was at control value. Similar results were observed for p62 and this can be explained because OPTN acts like a p62-like receptor<sup>29</sup>.

Combination chemotherapy of gemcitabine and *nab*-paclitaxel has been widely used in the treatment of advanced PC<sup>30,31</sup>. This drug combination showed comparable inhibition of FG cell viability with PAWI-2 alone (Supplemental Table S3; Fig. 3D). However, in FG $\beta_3$  cells, co-administration of gemcitabine and paclitaxel did not show significant enhancement on inhibition of cell viability compared to gemcitabine or paclitaxel alone (Fig. 3D). Drug resistance of this combination in FG $\beta_3$  cells was not associated with activated apoptosis because a comparable effect (activation on caspase activity and PARP cleavage for the combination compared to gemcitabine or paclitaxel alone; Supplemental Fig. S5A,B) was observed in both FG and FG $\beta_3$  cells. Synergism between gemcitabine and paclitaxel was associated with OPTN phosphorylation (Fig. 3E). OPTN phosphorylation may be linked to microtubule (MT) disturbance because this effect was also observed in paclitaxel (MT stabilizer)-treated cells (Fig. 3E).

**Effect of PAWI-2 and MT disturbance agents on cell cycle arrest.** PAWI-2 binds tubulin at the same site as colchicine<sup>22</sup>. Changes in pS177-OPTN and acetylation of tubulin (related to MT stabilization) as a function of PAWI-2 treatment in FG $\beta_3$  cells was evaluated (Fig. 4A). OPTN phosphorylation was correlated with tubulin acetylation and cell cycle arrest indicators (i.e., 4–6 fold decrease of cyclin D3 and 2–4 fold increase of p21 phosphorylation; Fig. 4A). For comparison, several well-defined MT disrupting agents (including MT stabilizers docetaxel and paclitaxel; MT destabilizers vinblastine and colchicine; Fig. 4B) confirmed this effect. Activation or inhibition of pS177-OPTN closely paralleled increase or inhibition of tubulin acetylation (Fig. 4B). Dose-dependent responses on OPTN phosphorylation or tubulin acetylation (Fig. 4C) by treatment with paclitaxel (activation of pS177-OPTN), PAWI-2 (MT stabilizer or destabilizer, dose-dependent changes on pS177-OPTN) and colchicine (inhibition of pS177-OPTN) was observed. However, inhibition of phosphorylation of TBK1 was only observed for PAWI-2 (Fig. 4B).

Double thymidine block arrests cells at the G1/S boundary and subsequent release to fresh media arrests cells at different boundaries<sup>32</sup>. Experiments were done to synchronize FG $\beta_3$  cells at the G1/S boundary and release upon treatment with vehicle control, PAWI-2 or paclitaxel (Fig. 4D). Activation of pS177-OPTN was detected at later G2/M phase (8 hours after release). This was closely associated with onset of cyclin D3 degradation and also inhibition of TBK1 phosphorylation (Fig. 4D). Similar results were observed for phosphorylation of p62 on Ser403 (pS403-p62). Based on intracellular distribution studies in FG $\beta_3$  cells, OPTN and pS177-OPTN (and also p62, NDP52) were mainly found in the cytoplasmic fraction under vehicle control conditions but accumulated in the nucleus with PAWI-2 (Fig. 4E). Accumulation of OPTN in the nuclear fraction was an indicator of G2/M arrest<sup>33</sup>. Cellular trafficking mediated by PAWI-2 was also associated with acetylated tubulin localization to nuclei (Fig. 4E). Similarly, nuclear cyclin D3 downregulation and accumulation of p21 (and its phosphorylated form) in cytoplasm were observed after administration of PAWI-2, paclitaxel or colchicine to FG $\beta_3$  cells (Fig. 4F), providing strong evidence that these MT disturbing agents caused FG $\beta_3$  cell G2/M arrest<sup>34,35</sup>. Together, these data show that PAWI-2 induced OPTN phosphorylation was highly associated with cell cycle arrest during mitosis.

## Discussion

We have shown that PAWI-2 could reverse cancer stemness and overcome drug resistance in an integrin  $\beta_3$  KRAS-dependent hPCSCs (i.e., FG $\beta_3$  cells). A working model of PAWI-2 was proposed (Fig. 5). In this model, OPTN plays a central role in regulation of TBK1 functional activity to reverse tumor stemness and drug resistance in FG $\beta_3$  cells. Phosphorylation of conserved OPTN residue (Ser177) by PAWI-2 promotes OPTN translocation

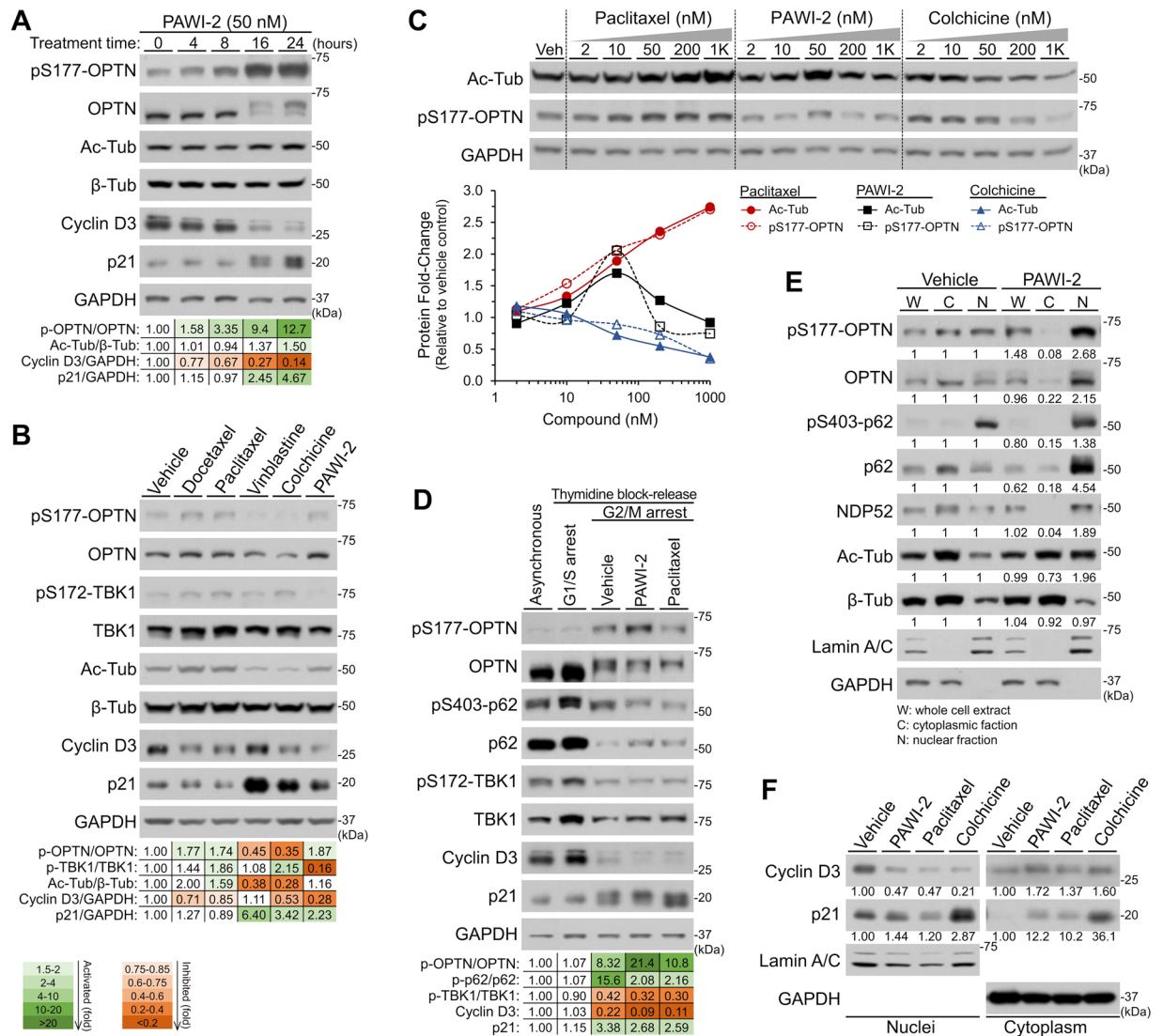


**Figure 4.** OPTN-dependent signaling controlled cell cycle arrest and the effect of PAWI-2 to overcome tumor stemness in FG $\beta_3$  cells. **(A)** Time-dependent effect of PAWI-2 on phosphorylation of OPTN (pS177-OPTN/OPTN) correlated with tubulin acetylation (Ac-Tub/ $\beta$ -Tub), cyclin D3 decrease and p21 phosphorylation. **(B)** The effect of MT disturbance agent (stabilizer: docetaxel, paclitaxel; destabilizer: vinblastine, colchicine) on pS177-OPTN, OPTN, pS172-TBK1, TBK1, Ac-Tub,  $\beta$ -Tub, cyclin D3 or p21 compared to PAWI-2 alone. **(C)** Dose-dependent response of paclitaxel, PAWI-2, or colchicine on pS177-OPTN and Ac-Tub. **(D)** FG $\beta_3$  cells arrested at the G1/S boundary with a double thymidine block and then released into fresh medium containing PAWI-2 or paclitaxel. Immunoblots and densitometry analysis of protein markers in G2/M arrest cells were done for comparison. **(E)** FG $\beta_3$  cells were fractionated into cytoplasmic (C) and nuclear (N) fractions. Immunoblots were conducted for indicated protein markers and compared to whole cell extracts (W). **(F)** The effect of PAWI-2, paclitaxel or colchicine on cytoplasmic accumulation of p21 and decrease of cyclin D3 in nuclear fractions. Concentrations of PAWI-2 used were as indicated: 50 nM in **A, B, D-F**, 2–1000 nM in **C**; concentrations of other MT disturbance agents used were as indicated: 50 nM in **B, D, F**, 2–1000 nM in **C**; treatment time used was as indicated: 0–24 hours in **A**, 8 hours in **B-F**; vehicle control (0.5% DMSO) in **GAPDH** was used as a loading control of whole cell extract in **A-D** and a marker of cytoplasmic fraction in **E, F**; Lamin A/C was used as a marker of the nuclear fraction in **E, F**. The full-length blots are presented in Supplementary Fig. S7.

into the nucleus and causes G2/M arrest. Concomitantly, OPTN phosphorylation induced by PAWI-2 has negative feedback control on TBK1 (dephosphorylation of TBK1 at S172) to inhibit dysregulation of KRAS-NF- $\kappa$ B signaling in FG $\beta_3$  cells. This model links a role of OPTN to the functional interplay between G2/M cell cycle arrest and provides a mechanism to explain how PAWI-2 overcomes tumor stemness.

Previously, we showed PAWI-2 activated DNA-damage checkpoint and mitochondrial p53-dependent apoptotic signaling in other non-CSC cancer cells<sup>22–24</sup>. Data herein showed this was also observed for hPSCs (FG $\beta_3$  cells). For dysregulated KRAS-RalB-NF- $\kappa$ B signaling in FG $\beta_3$  cells, galectin-3 plays a critical role in clustering

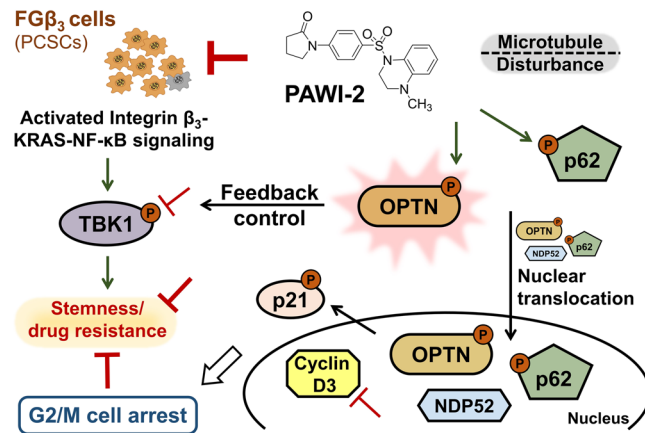


**Figure 5.** Proposed model depicts a mechanism of PAWI-2 to overcome tumor stemness and drug resistance in FG $\beta_3$  cells. Green arrows, stimulation; red lines, inhibition.

integrin  $\alpha_v\beta_3$  to induce KRAS and enable multiple processes in cancer cells<sup>21</sup>. In the study herein, PAWI-2 did not disrupt KRAS interactions with other effectors. This differentiates PAWI-2 from other drugs (e.g., GCS-100), that act as galectin-3 inhibitors and pharmacologically disrupt biochemical association between integrin  $\alpha_v\beta_3$  and KRAS<sup>21</sup>. RalA/B serves as molecular regulators of integrin  $\alpha_v\beta_3$ -KRAS-NF- $\kappa$ B signaling. PAWI-2 also did not measurably affect the inactive/active forms of RalA/B. These findings suggest that PAWI-2 inhibited KRAS-NF- $\kappa$ B signaling regardless of KRAS or Ral status. Given the fact that >90% of KRAS is activated by mutations in PC<sup>36</sup> and RAS or Ral inhibitors of these pathways have not proven effective clinically<sup>19</sup>, this suggests that PAWI-2 may possess advantages in clinical applications.

TBK1 is a serine/threonine kinase that is activated by autophosphorylation at Ser172 within the kinase activation loop<sup>37</sup>. Association of TBK1 with RalB of the major oncogene (RAS) in the integrin  $\alpha_v\beta_3$ -KRAS-NF- $\kappa$ B signaling pathway promotes tumorigenesis<sup>19,21</sup>. TBK1 inhibitors (e.g., momelotinib) show limited utility in PC even in combination with other effective PC therapeutics<sup>38</sup>. As a key kinase in several signaling pathways, TBK1 also phosphorylates p62 or OPTN to enhance their binding capacity with poly-ubiquitin (poly-UB) chains<sup>26,39</sup>. TBK1 constitutively interacts with OPTN to act as a key modulator to initiate elimination of damaged mitochondria via selective mitophagy (PINK1/Parkin-dependent mitophagy), that is involved in tumor suppression pathways<sup>40,41</sup>. PAWI-2 was previously reported to affect mitochondrial function (i.e., membrane trafficking, mitochondrial membrane potential changes)<sup>23,24</sup>. However, in FG $\beta_3$  cells neither PINK1 nor Parkin proteins were altered by PAWI-2. This data excludes mitophagy mechanisms initiated via OPTN by PAWI-2. PAWI-2 did not change autophagy biomarker LC3-I to lipidated form LC3-II (Supplemental Fig. S4C). Activation of OPTN phosphorylation by PAWI-2 may be related to other signaling cascades not solely dependent on TBK1. OPTN has also been shown to directly regulate TBK1<sup>42</sup>. A negative feedback control of TBK1 activation by OPTN helps explain the proposed working mechanism of PAWI-2. PAWI-2-induced OPTN phosphorylation negatively regulates TBK1 functional activity (i.e., autophosphorylation inhibited), and causes inhibition of KRAS-NF- $\kappa$ B signaling. This was further shown by exacerbated effects of PAWI-2 on the action of genetic knockdown of TBK1 and pharmacological inhibition (MRT67307) of TBK1 activation. Interestingly, MRT67307 does not affect accumulation of pS172-TBK1 (reversely activated). This shows that in contrast to previous reports<sup>27,43</sup>, TBK1 activation may not be the sole autocatalytic mechanism responsible operating for MRT67307.

In addition to being a downstream regulator of TBK1 function, OPTN is involved in a variety of other biological functions, including protection against apoptosis, Golgi organization, exocytosis, antiviral innate immune response, selective autophagy and other membrane trafficking mechanisms<sup>29,41</sup>. OPTN does not have any reported enzymatic activity but usually acts as an adaptor protein that links two different proteins (e.g., TBK1 and PINK1/Parkin)<sup>29,41</sup>. For tumorigenesis or tumor stemness, OPTN phosphorylation has been largely attributed to regulation of mitophagy<sup>44,45</sup> mediated by TBK1, but that was not observed herein for PAWI-2. Phosphorylation of OPTN at Ser177 also plays a pivotal role in mitotic progression and induces OPTN translocation into the nucleus<sup>46</sup>. OPTN-dependent G2/M cell cycle arrest induced by PAWI-2 in FG $\beta_3$  cells parallels this process. Previously, G2/M arrest was independently observed in PAWI-2-treated colon cancer cells<sup>22</sup>. This regulatory mechanism is abolished at the end of the G2/M phase as a consequence of nuclear translocation of OPTN and leads to increased activity of TBK1 (Supplemental Fig. S6).

Synergism between PAWI-2 and other validated drugs (i.e., erlotinib) was controlled by phosphorylation of OPTN. In contrast, in FG $\beta_3$  cells, if antagonism was observed (e.g., PAWI-2 with bortezomib), phosphorylation of OPTN was abolished. This observation helps explain drug resistance observed for FG $\beta_3$  cells treated with well-documented PC chemotherapies (e.g., gemcitabine with paclitaxel, Fig. 3E)<sup>30,31</sup>. OPTN may work as an over-arching branch-point for PAWI-2 inhibition of cell viability to overcome self-renewal capacity in FG $\beta_3$  cells and also to synergize other pathway inhibitors (i.e., erlotinib).

In PC cells, PAWI-2 binds to tubulin to stabilize/destabilize microtubules (MTs) and activate apoptotic signaling<sup>22–24</sup>. Phosphorylation of OPTN was closely associated with MT stabilization because this effect was also observed in cells treated with other MT stabilizers (e.g., paclitaxel or docetaxel; Fig. 4B). OPTN foci distribution



is dependent on the integrity of MTs<sup>46,47</sup>, but no relationship between OPTN phosphorylation and MT disturbance has been reported thus far. Nothing describing synergism between clinically-validated cancer drugs through regulation of OPTN has been reported. Accumulation of pS177-OPTN in the presence of MT stabilizers may be due to the essential role of MTs in coordinating and organizing many crucial cellular steps<sup>48</sup>. Thus, OPTN phosphorylation induced by PAWI-2 or other MT stabilizers could modulate synergism effects to overcome drug resistance and combat more aggressive CSCs.

In conclusion, PAWI-2 synergized specific pathway inhibitors (e.g., TBK1 inhibitors, EGFR inhibitors) against CSCs. Selective pharmacological potency of PAWI-2 in CSCs (e.g., FG $\beta_3$  cells versus FG cells) showed the utility of PAWI-2 to inhibit CSCs versus bulk cancer cells. This observation provides a basis for PAWI-2 as an efficient treatment of PC, especially in highly aggressive/metastatic cancer with stem-like properties and intrinsic or acquired drug resistance.

## Methods

**Cell lines.** FG and FG $\beta_3$  cells were provided by Dr. David Cheresch (UC San Diego and The Scripps Research Institute). FG $\beta_3$  cells have been thoroughly documented as an aggressive cell line showing CSC-like properties and cancer drug resistance<sup>19–21</sup>. FG and FG $\beta_3$  cells were grown in DMEM with 10% FBS. After thawing, cell lines were cultured at 37 °C in a humidified 5% CO<sub>2</sub> atmosphere and routinely screened for mycoplasma contamination.

**Compounds.** Synthesis and pharmaceutical properties of PAWI-2 (Fig. 1A) were reported previously<sup>25,49</sup>. Other drugs/inhibitors used in this study are listed in the Supplementary Materials and Methods.

**Cell viability and apoptosis assays.** FG and FG $\beta_3$  cells were seeded onto plates and treated with test compounds (vehicle, 0.5% DMSO; PAWI-2 or other drugs; 2 to 5000 nM) for 3 days. Cell viability was determined using CellTiter-Glo (Promega). Data were expressed as percentage of survival compared to survival of vehicle-treated cells. A similar protocol was used to test synergy of PAWI-2 in the presence of erlotinib and/or bortezomib. Chou-Talalay analysis used commercial software (ComboSyn)<sup>50</sup>. Cell apoptosis was determined by quantifying caspase-3/7 activity using Caspase-Glo 3/7 (Promega).

**Tumor-sphere culture and self-renewal assay.** FG and FG $\beta_3$  cells were seeded on ultra-low attachment plates at single-cell suspensions (1,000 cells ml<sup>-1</sup>) in DMEM/F12 medium containing insulin-transferrin-selenium (Corning) supplemented with EGF and bFGF (Gibco). Primary tumor spheres were formed after 7 days. Cells were then treated with test compounds for 24 hours. Primary tumor spheres larger than 50  $\mu$ m in diameter were counted for each condition in triplicate. Single-cell suspensions were dissociated from primary tumor spheres by filtration through a 40  $\mu$ m cell strainer and seeded using the same conditions. Secondary tumor spheres were formed after 7 days and treated and counted similarly as that for primary tumor spheres.

**Subcellular fractionation, immunoprecipitation and immunoblotting.** Subcellular fractionation and immunoblot experiments were carried out as before<sup>24</sup>. Whole-cell extracts were obtained after lysis with RIPA buffer (Supplementary Materials and Methods) and subcellular fractions were obtained after homogenization in isolation buffer and centrifugation. Immunoprecipitation experiments were carried out as before with specific antibodies<sup>24</sup>. Protein extracts were resolved by SDS-PAGE followed by immunoblotting using antibodies specific for target proteins (Supplementary Materials and Methods). Densities of immunoblot bands were quantified using ImageJ (NIH).

**Genetic knockdown.** FG and FG $\beta_3$  cells were transfected with TBK1 small hairpin RNA (shRNA; Dharmacon; Supplementary Table S4) using lipofectamine 3000 reagent (Invitrogen). Gene knockdown was confirmed by immunoblotting.

**Ral activation assay.** Affinity pulldown assays for RalA/B were carried out following manufacturer's instructions (Cell Biolabs). Cells were cultured in suspension and treated with vehicle or PAWI-2 (50 nM) for 8 hours. Lysate obtained was incubated with RalBP1 PBD agarose bead slurry at 4 °C for 1 hour with gentle agitation. Activated forms of Ral (GTP bound) bound to beads were collected, washed and resolved by SDS-PAGE followed by immunoblotting using RalA/B antibodies.

**Double thymidine block and release.** FG $\beta_3$  cells were first incubated with 2 mM thymidine (Sigma) for 18 hours and released into fresh medium for 8 hours. Thymidine treatment was repeated, and a second release was conducted for 0–8 hours by releasing cells for treatment with vehicle, PAWI-2 or paclitaxel. For G1/S boundary, cells were collected at 0 hour. For the G2/M boundary studies, cells were collected at 8 hours for analysis of protein by immunoblots.

**Statistical analysis.** IC<sub>50</sub> and EC<sub>50</sub> values were calculated using a nonlinear regression analysis (GraphPad Prism) of the mean and standard deviation (SD) or standard error of the mean (SEM) of at least triplicate samples for each biological assay. Student *t* tests were used to calculate statistical significance and a *P*-value < 0.05 was considered significant.

Received: 3 March 2020; Accepted: 11 May 2020;

Published online: 08 June 2020

## References

- Rahib, L. *et al.* Projecting cancer incidence and deaths to 2030: the unexpected burden of thyroid, liver, and pancreas cancers in the United States. *Cancer Res.* **74**, 2913–2921, <https://doi.org/10.1158/0008-5472.CAN-14-0155> (2014).
- Siegel, R. L., Miller, K. D. & Jemal, A. Cancer Statistics, 2018. *CA Cancer J. Clin.* **68**, 7–30, <https://doi.org/10.3322/caac.21387> (2018).
- Oettle, H. *et al.* Adjuvant chemotherapy with gemcitabine vs observation in patients undergoing curative-intent resection of pancreatic cancer: a randomized controlled trial. *JAMA* **297**, 267–277, <https://doi.org/10.1001/jama.297.3.267> (2007).
- Ansari, D. *et al.* Pancreatic cancer: yesterday, today and tomorrow. *Future Oncol.* **12**, 1929–1946, <https://doi.org/10.2217/fon-2016-0010> (2016).
- Burris, H. A. 3rd *et al.* Improvements in survival and clinical benefit with gemcitabine as first-line therapy for patients with advanced pancreas cancer: a randomized trial. *J. Clin. Oncol.* **15**, 2403–2413, <https://doi.org/10.1200/jco.1997.15.6.2403> (1997).
- Conroy, T. *et al.* FOLFIRINOX versus gemcitabine for metastatic pancreatic cancer. *N. Engl. J. Med.* **364**, 1817–1825, <https://doi.org/10.1056/NEJMoa1011923> (2011).
- Conroy, T., Gavaille, C. & Adenis, A. Metastatic pancreatic cancer: old drugs, new paradigms. *Curr. Opin. Oncol.* **23**, 390–395, <https://doi.org/10.1097/CCO.0b013e3283473610> (2011).
- Hanahan, D. & Weinberg, R. A. Hallmarks of cancer: the next generation. *Cell* **144**, 646–674, <https://doi.org/10.1016/j.cell.2011.02.013> (2011).
- Meacham, C. E. & Morrison, S. J. Tumour heterogeneity and cancer cell plasticity. *Nature* **501**, 328–337, <https://doi.org/10.1038/nature12624> (2013).
- Dean, M., Fojo, T. & Bates, S. Tumour stem cells and drug resistance. *Nat. Rev. Cancer* **5**, 275–284, <https://doi.org/10.1038/nrc1590> (2005).
- Hermann, P. C. *et al.* Distinct populations of cancer stem cells determine tumor growth and metastatic activity in human pancreatic cancer. *Cell Stem Cell* **1**, 313–323, <https://doi.org/10.1016/j.stem.2007.06.002> (2007).
- Kreso, A. & Dick, J. E. Evolution of the cancer stem cell model. *Cell Stem Cell* **14**, 275–291, <https://doi.org/10.1016/j.stem.2014.02.006> (2014).
- Nassar, D. & Blanpain, C. Cancer Stem Cells: Basic Concepts and Therapeutic Implications. *Annu. Rev. Pathol.* **11**, 47–76, <https://doi.org/10.1146/annurev-pathol-012615-044438> (2016).
- Desgrosellier, J. S. & Cheresch, D. A. Integrins in cancer: biological implications and therapeutic opportunities. *Nat. Rev. Cancer* **10**, 9–22, <https://doi.org/10.1038/nrc2748> (2010).
- Adhikari, A. S., Agarwal, N. & Iwakuma, T. Metastatic potential of tumor-initiating cells in solid tumors. *Front. Biosci.* **16**, 1927–1938 (2011).
- Miller, P. G. *et al.* *In Vivo* RNAi screening identifies a leukemia-specific dependence on integrin beta 3 signaling. *Cancer Cell* **24**, 45–58, <https://doi.org/10.1016/j.ccr.2013.05.004> (2013).
- Vaillant, F. *et al.* The mammary progenitor marker CD61/beta3 integrin identifies cancer stem cells in mouse models of mammary tumorigenesis. *Cancer Res.* **68**, 7711–7717, <https://doi.org/10.1158/0008-5472.CAN-08-1949> (2008).
- Bivona, T. G. *et al.* FAS and NF-kappaB signalling modulate dependence of lung cancers on mutant EGFR. *Nature* **471**, 523–526, <https://doi.org/10.1038/nature09870> (2011).
- Seguin, L. *et al.* An integrin beta(3)-KRAS-RalB complex drives tumour stemness and resistance to EGFR inhibition. *Nat. Cell Biol.* **16**, 457–468, <https://doi.org/10.1038/ncb2953> (2014).
- Desgrosellier, J. S. *et al.* An integrin alpha(v)beta(3)-c-Src oncogenic unit promotes anchorage-independence and tumor progression. *Nat. Med.* **15**, 1163–1169, <https://doi.org/10.1038/nm.2009> (2009).
- Seguin, L. *et al.* Galectin-3, a Druggable Vulnerability for KRAS-Addicted Cancers. *Cancer Discov.* **7**, 1464–1479, <https://doi.org/10.1158/2159-8290.CD-17-0539> (2017).
- Cheng, J., Dwyer, M., Okolotowicz, K. J., Mercola, M. & Cashman, J. R. A Novel Inhibitor Targets Both Wnt Signaling and ATM/p53 in Colorectal Cancer. *Cancer Res.* **78**, 5072–5083, <https://doi.org/10.1158/0008-5472.CAN-17-2642> (2018).
- Cheng, J. *et al.* A Novel Small Molecule Inhibits Tumor Growth and Synergizes Effects of Enzalutamide on Prostate Cancer. *J. Pharmacol. Exp. Ther.* **371**, 703–712, <https://doi.org/10.1124/jpet.119.261040> (2019).
- Cheng, J. *et al.* Inhibition of invasive pancreatic cancer: restoring cell apoptosis by activating mitochondrial p53. *Am. J. Cancer Res.* **9**, 390–405 (2019).
- Okolotowicz, K. J. *et al.* Novel tertiary sulfonamides as potent anti-cancer agents. *Bioorg Med. Chem.* **26**, 4441–4451, <https://doi.org/10.1016/j.bmc.2018.07.042> (2018).
- Wild, P. *et al.* Phosphorylation of the autophagy receptor optineurin restricts Salmonella growth. *Science* **333**, 228–233, <https://doi.org/10.1126/science.1205405> (2011).
- Clark, K. *et al.* Novel cross-talk within the IKK family controls innate immunity. *Biochem. J.* **434**, 93–104, <https://doi.org/10.1042/BJ20101701> (2011).
- Kao, C. *et al.* Bortezomib enhances cancer cell death by blocking the autophagic flux through stimulating ERK phosphorylation. *Cell Death Dis.* **5**, e1510, <https://doi.org/10.1038/cddis.2014.468> (2014).
- Kachaner, D., Genin, P., Laplantine, E. & Weil, R. Toward an integrative view of Optineurin functions. *Cell Cycle* **11**, 2808–2818, <https://doi.org/10.4161/cc.20946> (2012).
- Frese, K. K. *et al.* nab-Paclitaxel potentiates gemcitabine activity by reducing cytidine deaminase levels in a mouse model of pancreatic cancer. *Cancer Discov.* **2**, 260–269, <https://doi.org/10.1158/2159-8290.CD-11-0242> (2012).
- Von Hoff, D. D. *et al.* Gemcitabine plus nab-paclitaxel is an active regimen in patients with advanced pancreatic cancer: a phase I/II trial. *J. Clin. Oncol.* **29**, 4548–4554, <https://doi.org/10.1200/JCO.2011.36.5742> (2011).
- Ma, H. T. & Poon, R. Y. Synchronization of HeLa Cells. *Methods Mol. Biol.* **1524**, 189–201, [https://doi.org/10.1007/978-1-4939-6603-5\\_12](https://doi.org/10.1007/978-1-4939-6603-5_12) (2017).
- Delaval, B. *et al.* Aurora B -TACC1 protein complex in cytokinesis. *Oncogene* **23**, 4516–4522, <https://doi.org/10.1038/sj.onc.1207593> (2004).
- Dash, B. C. & El-Deiry, W. S. Phosphorylation of p21 in G2/M promotes cyclin B-Cdc2 kinase activity. *Mol. Cell Biol.* **25**, 3364–3387, <https://doi.org/10.1128/MCB.25.8.3364-3387.2005> (2005).
- Heliez, C., Baricault, L., Barboulet, N. & Valette, A. Paclitaxel increases p21 synthesis and accumulation of its AKT-phosphorylated form in the cytoplasm of cancer cells. *Oncogene* **22**, 3260–3268, <https://doi.org/10.1038/sj.onc.1206409> (2003).
- Deer, E. L. *et al.* Phenotype and genotype of pancreatic cancer cell lines. *Pancreas* **39**, 425–435, <https://doi.org/10.1097/MPA.0b013e3181c15963> (2010).
- Ma, X. *et al.* Molecular basis of Tank-binding kinase 1 activation by transautophosphorylation. *Proc. Natl Acad. Sci. USA* **109**, 9378–9383, <https://doi.org/10.1073/pnas.1121552109> (2012).
- Ng, K. *et al.* Phase 1 dose-escalation study of momelotinib, a Janus kinase 1/2 inhibitor, combined with gemcitabine and nab-paclitaxel in patients with previously untreated metastatic pancreatic ductal adenocarcinoma. *Invest. N. Drugs* **37**, 159–165, <https://doi.org/10.1007/s10637-018-0650-5> (2019).
- Pilli, M. *et al.* TBK-1 promotes autophagy-mediated antimicrobial defense by controlling autophagosome maturation. *Immunity* **37**, 223–234, <https://doi.org/10.1016/j.immuni.2012.04.015> (2012).
- Richter, B. *et al.* Phosphorylation of OPTN by TBK1 enhances its binding to Ub chains and promotes selective autophagy of damaged mitochondria. *Proc. Natl Acad. Sci. USA* **113**, 4039–4044, <https://doi.org/10.1073/pnas.1523926113> (2016).

41. Weil, R., Laplantine, E., Curic, S. & Genin, P. Role of Optineurin in the Mitochondrial Dysfunction: Potential Implications in Neurodegenerative Diseases and Cancer. *Front. Immunol.* **9**, 1243, <https://doi.org/10.3389/fimmu.2018.01243> (2018).
42. Pourcelot, M. *et al.* The Golgi apparatus acts as a platform for TBK1 activation after viral RNA sensing. *BMC Biol.* **14**, 69, <https://doi.org/10.1186/s12915-016-0292-z> (2016).
43. Heo, J. M., Ordureau, A., Paulo, J. A., Rinehart, J. & Harper, J. W. The PINK1-PARKIN Mitochondrial Ubiquitylation Pathway Drives a Program of OPTN/NDP52 Recruitment and TBK1 Activation to Promote Mitophagy. *Mol. Cell* **60**, 7–20, <https://doi.org/10.1016/j.molcel.2015.08.016> (2015).
44. Liu, K. *et al.* Mitophagy Controls the Activities of Tumor Suppressor p53 to Regulate Hepatic Cancer Stem Cells. *Mol. Cell* **68**(281–292), e285, <https://doi.org/10.1016/j.molcel.2017.09.022> (2017).
45. Liu, Z. *et al.* Ubiquitylation of autophagy receptor Optineurin by HACE1 activates selective autophagy for tumor suppression. *Cancer Cell* **26**, 106–120, <https://doi.org/10.1016/j.ccr.2014.05.015> (2014).
46. Ying, H., Shen, X., Park, B. & Yue, B. Y. Posttranslational modifications, localization, and protein interactions of optineurin, the product of a glaucoma gene. *PLoS One* **5**, e9168, <https://doi.org/10.1371/journal.pone.0009168> (2010).
47. Park, B. C., Shen, X., Samaraweera, M. & Yue, B. Y. Studies of optineurin, a glaucoma gene: Golgi fragmentation and cell death from overexpression of wild-type and mutant optineurin in two ocular cell types. *Am. J. Pathol.* **169**, 1976–1989, <https://doi.org/10.2353/ajpath.2006.060400> (2006).
48. Brouhard, G. J. & Rice, L. M. Microtubule dynamics: an interplay of biochemistry and mechanics. *Nat. Rev. Mol. Cell Biol.* **19**, 451–463, <https://doi.org/10.1038/s41580-018-0009-y> (2018).
49. Cashman, J. R., Mercola, M., Schade, D. & Tsuda, M. Compounds for inhibition of cancer cell proliferation. *Google Patents*, US 13/748,770 (2013).
50. Chou, T. C. Drug combination studies and their synergy quantification using the Chou-Talalay method. *Cancer Res.* **70**, 440–446, <https://doi.org/10.1158/0008-5472.CAN-09-1947> (2010).

## Acknowledgements

We thank Dr. David Cheresch of the University of California, San Diego and The Scripps Research Institute for FG and FG<sub>3</sub> cells. This work was supported by Inception Award from California Institute for Regenerative Medicine (CIRM) (DISC1–10583; J.R. Cashman) and by funds from the Human BioMolecular Research Institute. The contents of this publication are solely the responsibility of the authors and do not necessarily represent the official view of CIRM or any other agency of the State of California.

## Author contributions

J.C. and J.R.C. conceived the study. J.C. conducted and carried out all the cell-based studies, data analysis and statistical analysis. All authors contributed to drafting and revising the manuscript. All authors approved the manuscript.

## Competing interests

The authors declare no competing interests.

## Additional information

**Supplementary information** is available for this paper at <https://doi.org/10.1038/s41598-020-65804-5>.

**Correspondence** and requests for materials should be addressed to J.C.

**Reprints and permissions information** is available at [www.nature.com/reprints](http://www.nature.com/reprints).

**Publisher's note** Springer Nature remains neutral with regard to jurisdictional claims in published maps and institutional affiliations.



**Open Access** This article is licensed under a Creative Commons Attribution 4.0 International License, which permits use, sharing, adaptation, distribution and reproduction in any medium or format, as long as you give appropriate credit to the original author(s) and the source, provide a link to the Creative Commons license, and indicate if changes were made. The images or other third party material in this article are included in the article's Creative Commons license, unless indicated otherwise in a credit line to the material. If material is not included in the article's Creative Commons license and your intended use is not permitted by statutory regulation or exceeds the permitted use, you will need to obtain permission directly from the copyright holder. To view a copy of this license, visit <http://creativecommons.org/licenses/by/4.0/>.

© The Author(s) 2020